CHIN. PHYS. LETT. Vol. 33, No. 10 (2016) 107501

Controllable Synthesis and Magnetic Properties of Monodisperse Fe_3O_4 Nanoparticles *

Zhu-Liang Wang(王朱良), Hui Ma(马慧), Fang Wang(王芳)**, Min Li(李敏), Li-Guo Zhang(张利国), Xiao-Hong Xu(许小红)**

Key Laboratory of Magnetic Molecules and Magnetic Information Material (Ministry of Education), School of Chemistry and Materials Science, Shanxi Normal University, Linfen 041004

(Received 2 June 2016)

Magnetite (Fe_3O_4) nanoparticles with different sizes and shapes are synthesized by the thermal decomposition method. Two approaches, non-injection one-pot and hot-injection methods, are designed to investigate the growth mechanism in detail. It is found that the size and shape of nanoparticles are determined by adjusting the precursor concentration and duration time, which can be well explained by the mechanism based on the LaMer model in our synthetic system. The monodisperse Fe_3O_4 nanoparticles have a mean diameter from 5 nm to 16 nm, and shape evolution from spherical to triangular and cubic. The magnetic properties are size-dependent, and Fe_3O_4 nanoparticles in small size about 5 nm exhibit superparamagnetic properties at room temperature and maximum saturation magnetization approaches to 78 emu/g, whereas Fe_3O_4 nanoparticles develop ferromagnetic properties when the diameter increases to about 16 nm.

PACS: 75.47.Lx, 81.07.−b, 81.10.Dn, 81.16.Be DOI: 10.1088/0256-307X/33/10/107501

Fe_3O_4 is an important kind of magnetic material having a cubic inverse spinel structure with oxygen anions forming a face-centered-cubic (FCC) close-packed structure, which has been of scientific and technological interest in recent years. Due to their low toxicity, innate biocompatibility, high saturation magnetization, and room temperature superparamagnetism under critical size, Fe_3O_4 nanoparticles can be used in magnetic resonance imaging (MRI) contrast enhancement,[1−4] catalysis,[5−7] magnetic separation,[8−11] ferrofluids,[12,13] controlled drug delivery,[14,15] biosensor and medical diagnosis, etc.[16−18] The magnetic properties of Fe_3O_4 nanoparticles can be tailored by controlling the size, shape, crystallinity, and monodispersity in synthesizing and assembling, which is important for exploring their growth process and mechanism.

For these reasons, many efforts were focused on controlling the shape and size by changing the synthesis conditions. Sun *et al.* reported that high-temperature reaction of $Fe(acac)_3$ in the presence of alcohol, oleic acid, and oleylamine could be used to produce size-controlled monodisperse Fe_3O_4 nanoparticles.[19] Ho *et al.* investigated shape-controlled growth and shape-dependent cation site occupancy of monodisperse Fe_3O_4 nanoparticles by a modified hot-injection method.[20] Li *et al.* synthesized hexagonal and triangular monodisperse Fe_3O_4 nanosheets enclosed by {111} planes through a two-step microemulsion solvothermal process.[21] Although great efforts are given, it is still necessary to systematically study the size- and shape-evolution process and mechanisms of Fe_3O_4 nanoparticles.

In this work, spherical, polyhedral, triangular, and cubic Fe_3O_4 nanoparticles are synthesized by using non-injection one-pot and hot-injection methods, and the size and shape evolution are systematically investigated by controlling the synthesis conditions. The results show that the size and shape of Fe_3O_4 nanoparticles strongly depend on precursor concentration, nucleation and growth time, and affect magnetic properties, which is promising to controllably synthesize Fe_3O_4 and to clarify its growth mechanism and potential applications.

The chemical reagents used in our work were iron (Ⅲ) acetylacetonate ($Fe(acac)_3$), oleylamine, oleic acid, benzy ether, 1,2-hexadecanediol and n-hexane. All of the reagents were analytical grade. The synthesis was carried out by using the typical thermal decomposition method under the protection of nitrogen. We designed two routes, non-injection one-pot and hot-injection methods, to control the grain size and crystal shape. In the non-injection one-pot method, $Fe(acac)_3$, oleylamine, benzy ether were mixed in a four-neck flask. Then the mixture was heated to 120℃ with constant magnetic stirring under the protection of nitrogen. After maintaining the temperature for about 30 min, the mixture was heated to 300℃, and refluxed for a certain time to obtain Fe_3O_4 nanoparticles. In the hot-injection method, $Fe(acac)_3$ and

*Supported by the National Natural Science Foundation of China under Grant Nos 51571135, 11274214 and 61434002, the Special Funds of Shanxi Scholars Program under Grant No IRT1156, Collaborative Innovation Center for Shanxi Advanced Permanent Materials and Technology, and the Special Funds of the Ministry of Education of China under Grant No 20121404130001.

**Corresponding author. Email: wf_0716@163.com; xuxiaohong_ly@163.com

© 2016 Chinese Physical Society and IOP Publishing Ltd

benzyl ether were mixed as precursor solution in advance, 0.2 M $Fe(acac)_3$ precursor solution was used in our work. Oleylamine or 1,2-hexadecanediol solution was used as the background solution in a four-neck flask. The background solution was heated to 120℃ with constant magnetic stirring under the protection of nitrogen, maintaining the temperature for about 30 min, further heated to 300℃. Then the precursor solution was injected into the flask by controlling injection rate of 10 ml/h, and reflux for 2 h to obtain Fe_3O_4 nanoparticles. The flask was cooled to room temperature naturally after both non-injection one-pot and hot-injection methods. The black precipitate was washed with n-hexane and ethanol, and separated by centrifugation (4500 rpm) several times. The collected Fe_3O_4 nanoparticles were finally dried in a desiccator at 60℃ for 4 h for further characterization.

The size and morphology were observed by a transmission electron microscope (TEM JEM-2100). The crystalline structure of the nanoparticles was characterized by x-ray diffraction (XRD Rigaku Ultima Ⅳ). The magnetic measurement was carried out by a vibrating sample magnetometer (VSM Lakeshore 7407) and a superconducting quantum interference device (SQUID MPMS-XL-5).

All the TEM images in our work show that the decomposition reaction of $Fe(acac)_3$ at high temperature can lead to monodisperse nanoparticles. To understand the formation mechanism of monodisperse nanoparticles in the non-injection one-pot method, we change firstly the amount of $Fe(acac)_3$ precursors but fix oleylamine, benzyl oxide, and reaction time. Then we change the reaction time but fix the amount of $Fe(acac)_3$ precursors, oleylamine and benzyl oxide.

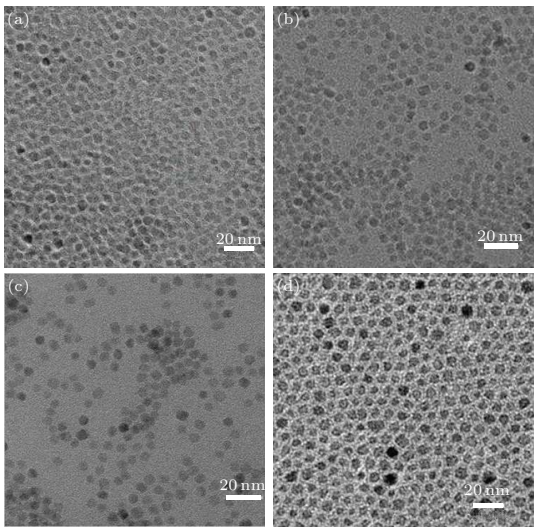


Fig. 1. TEM images of nanoparticles made by the non-injection one-pot method for the amounts of $Fe(acac)_3$ precursor: (a) 0.5 mmol, (b) 1 mmol, (c) 2 mmol and (d) 4 mmol.

Figure 1 shows the size and shape of Fe_3O_4 nanoparticles obtained at different amounts of $Fe(acac)_3$ precursor while fixing oleylamine at 30 ml, benzyl oxide 10 ml, and reaction time 1 h. As for the TEM images shown in Fig. 1, when the amount of $Fe(acac)_3$ precursors increases from 0.5 mmol to 2 mmol, only slight increase is observed in the size of nanopraticles, the mean size of nanoparticles is increased from ∼4.5 nm to ∼5 nm. When the amount of $Fe(acac)_3$ precursors increases from 2 mmol to 4 mmol, the mean size of nanoparticles is obviously increased from ∼5 nm to ∼7 nm. The formation mechanism of Fe_3O_4 monodisperse nanoparticles might be explained by the LaMer model.[22] According to the LaMer model, the particles formation process includes three periods. In period I, the concentration of monomers generated from $Fe(acac)_3$ precursors is gradually increased and reaches the minimum nucleation concentration, namely the critical supersaturation level (C_{crit}). In period Ⅱ, the nucleation occurs and nanoparticles grow, and then the monomer concentration is decreased to C_{crit}. In period Ⅲ, the monomer concentration is gradually decreased for further growth of nanoparticles.

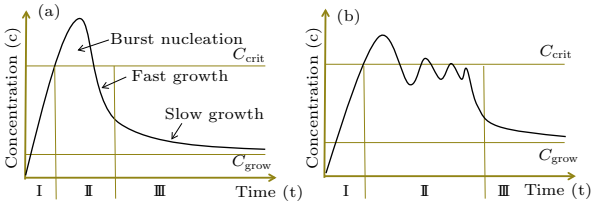


Fig. 2. Schematic illustration of nucleation and growth mechanisms based on the LaMer model: (a) mechanism for the non-injection one-pot method, and (b) mechanism for the hot-injection method.

Figure 2(a) shows the formation schematic illustration of the non-injection one-pot method based on the LaMer model, it has only one fluctuation in period Ⅱ, which means that only one burst nucleation occurs in the process of formation nanoparticles. In the non-injection one-pot method, when the monomer concentration generated by $Fe(acac)_3$ precursors is above C_{crit}, then burst nucleation occurs and the nanoparticles would be formed rapidly to a critical size. After burst nucleation, the remaining monomers grow on the existing nuclei. When the amount of $Fe(acac)_3$ precursors is low in a certain volume, 0.5–2 mmol in our system, the large monomers generated by $Fe(acac)_3$ precursors are consumed first to form crystal nuclei, only a small number of monomers will be used to enlarge the nanoparticles, thus there is only slight increase in the size of nanoparticles. However, when the amount of $Fe(acac)_3$ precursors is high in a certain volume, exceeding 2 mmol in our system, there are more monomers growing on the existing nuclei after burst nucleation, which leads to larger size.

The shape variations of Fe_3O_4 nanoparticles de-

pending on the amount of $Fe(acac)_3$ precursors are also observed from the TEM images in Fig. 1. The nanoparticle shapes should be determined by the facet growth rates of Fe_3O_4 nanoparticles, which might be governed by the intrinsic surface energy and the monomer concentration in our system. As shown in Fig. 1, when the amount of $Fe(acac)_3$ precursor is 0.5–2 mmol, the monomer concentration is low in the period Ⅱ, the amount of monomers growing on existing nuclei is small after burst nucleation, leading to slight changes in shapes of nanoparticles. However, when the amount of $Fe(acac)_3$ precursors is high, 4 mmol in our system, the monomer concentration is high in the period Ⅱ, more monomers grow at different planes by different rates, leading to irregular polyhedral shapes.

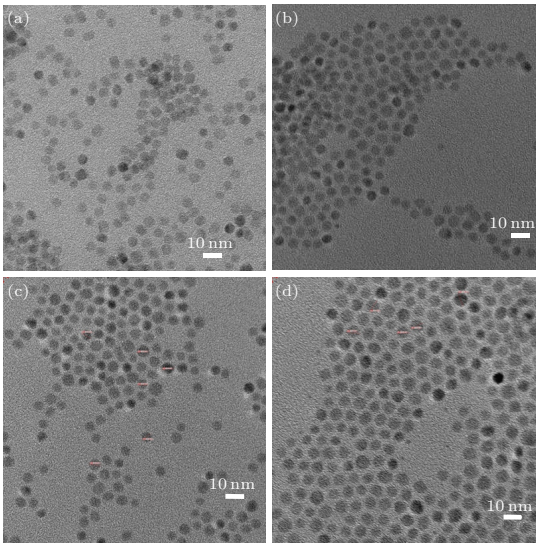


Fig. 3. TEM images of nanoparticles prepared by the non-injection one-pot method at different reaction durations: (a) 1 h, (b) 2 h, (c) 3 h, and (d) 4 h.

Figure 3 shows the size and shape of Fe_3O_4 nanoparticles obtained by the non-injection one-pot method at different reaction durations with fixed $Fe(acac)_3$ precursors at 2 mmol, oleylamine 30 ml, benzyl oxide 10 ml. As shown in Fig. 3, the mean size of nanoparticles increases from ∼5 nm to ∼7 nm along with the reaction time increases from 1 h to 4 h, which shows that extending reaction time can increase the size of nanoparticles. This might be due to the fact that, in period Ⅲ of the LaMer model, the monomer concentration is gradually decreased for further growth of nanoparticles and Oswald ripening.[23] The increase rate affected by duration time, 2 nm in 3 h, is much lower than that of changing the amount of $Fe(acac)_3$ precursors in our system, at least 4.5 nm in the first one hour. This indicates that the growth of nanoparticles at this period is a slow process. It is also noticed that the shape of nanoparticles has no obvious variation by changing duration time from 1 h to 4 h. This means that the influence on shape of the nanoparticles is slight in period Ⅲ of the LaMer model compared with that in period Ⅱ in our system.

According to the above discussion, it is deduced that period Ⅱ of the LaMer model is crucial for controlling the size and shape in our synthetic system. This mechanism is somewhat different when contrasted to the shape formation mechanism of Ho *et al.*[20] who proposed that the final shape of Fe_3O_4 nanoparticles is determined in period Ⅲ of the LaMer model. To further discuss the growth mechanism of nanoparticles, we use the hot-injection method to extend the burst nucleation and fast growth time in period Ⅱ by controlling the monomer concentration. Here 0.2 M $Fe(acac)_3$ precursor solution is injected slowly into different background solutions. The formation process of the hot-injection method can be described by a modified schematic illustration based on the LaMer model (shown in Fig. 2(b)).

The TEM images of Fe_3O_4 nanoparticles made in the hot-injection method are shown in Figs. 4(a) (oleylamine as background solution) and 4(b) (1,2-hexadecanediol solution as background solution). As shown in Fig. 4, the size and shape of Fe_3O_4 nanoparticles made in hot-injection are very different from those made by the non-injection one-pot method, the size of Fe_3O_4 nanoparticles in hot-injection is greatly larger than that by the non-injection one-pot method using the same dosage of $Fe(acac)_3$ precursors at 2 mmol, and the shapes of Fe_3O_4 nanoparticles are triangle and cubic, more regular than those using the non-injection one-pot method.

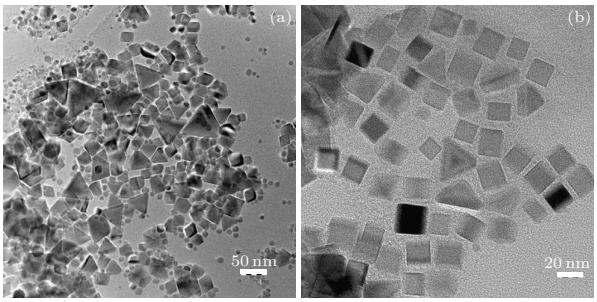


Fig. 4. TEM images of nanoparticles made by the hot-injection method (a) oleylamine solution as background and (b) 1, 2-hexadecanediol solution as background.

As illustrated in Fig. 2(b), compared with the non-injection one-pot method, the hot-injection method can control the concentrations of $Fe(acac)_3$ precursor by slowly injecting, and this allows an extended nucleation and fast growth period. The rate of injection determines the amount of nanoparticles per unit time in the reaction. The hot-injection method with slow rate avoids large-scale nucleation fluctuation and allows monomers to grow on the existing nuclei, which helps to form larger-sized nanoparticles.

We also notice that the particles in Fig. 4(a) exhibit broader size compared with that of parti-

cles in Fig. 4(b), maybe due to the fact that the reducibility of oleylamine is stronger than that of 1,2-hexadecanediol,[24] and the monomers generated in oleylamine solution are more than those in 1,2-hexadecanediol solution per unit time, which provides more larger fluctuations around $C_{\rm crit}$ in period Ⅱ of the LaMer model. Therefore, at the same injection rate in our system, multiple nucleation events may happen in oleylamine background solution, the sizes of nanoparticles formed in the first burst nucleation are larger than those in the later burst nucleation, leading to broader size distribution. Only a single burst nucleation event may happen in 1,2-hexadecanediol background solution, then the monomer concentration is kept below $C_{\rm crit}$, the remaining monomers generated with injection might grow on the existing nuclei, leading to relative narrow size distribution.

For spinel oxides, the {100} facet shows the lowest surface energy while the {111} facet has the highest one among {100}, {110} and {111} facets.[25] The stronger reductant can make more monomers in the same injection rate, leading to a higher concentration of burst nucleation than that of weak reductant. When the concentration of burst nucleation is high, the energy of monomers is large. Therefore the triangle nanoparticles with the highest surface energy {111} can be easily formed in oleylamine solution. When the concentration of burst nucleation is low, the energy of monomers is small, the cubic nanoparticles with lowest surface energy {100} can be inclined to form in 1,2-hexadecanediol solution. Appearance of a few triangle nanoparticles may be due to local inhomogeneity in the injecting process which makes some triangle nanoparticles with high energy {111} still remain. This indicates that the shapes of nanoparticles can be controlled by the rate of the injection.

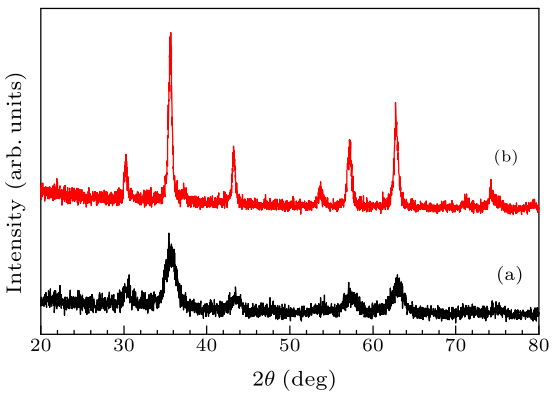


Fig. 5. X-ray diffraction patterns of (a) ∼5 nm Fe_3O_4 nanoparticles made by the non-injection one-pot method, and (b) ∼16 nm Fe_3O_4 nanoparticles made by the hot-injection method.

X-ray diffraction patterns of small size (∼5 nm) made by the non-injection one-pot method and large size (∼16 nm) made by the hot-injection method are shown in Fig. 5. The position and relative intensity of all diffraction peaks can match well with face-centered Fe_3O_4 (JCPDS No. 65-3107), indicating that Fe_3O_4 nanoparticles made by the non-injection one-pot or hot-injection method are single crystal without impurity phases. It is observed that the widths of reflection peaks become sharper with the increase of the size, which is consistent with Scherrer's formula. We can also observe that the intensity of peaks in ∼16 nm Fe_3O_4 nanoparticles is greatly higher than that in ∼5 nm Fe_3O_4 nanoparticles, indicating that the crystallinity of Fe_3O_4 nanoparticles tends to improve.

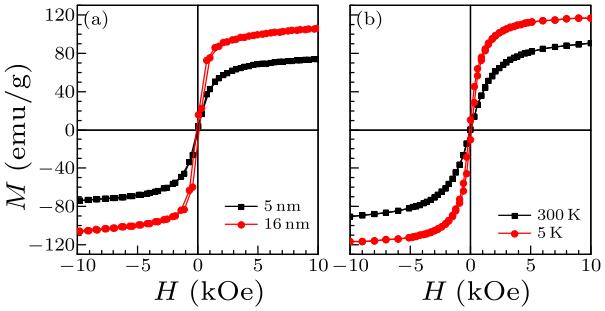


Fig. 6. Hysteresis loops of (a) ∼5 nm and ∼16 nm Fe_3O_4 nanoparticles measured by VSM at room temperature and (b) ∼5 nm Fe_3O_4 nanoparticles measured by SQUID at 5 K and 300 K.

Figure 6(a) shows the hysteresis loops of small size (∼5 nm) Fe_3O_4 nanoparticles and large size Fe_3O_4 nanoparticles (∼16 nm) measured by VSM at room temperature. For Fe_3O_4 nanoparticles, it is noticed that the saturation magnetization values depend on the size of the particles. The saturation magnetization values of Fe_3O_4 particles are 78 emu/g and 110 emu/g when their sizes are ∼5 nm and ∼16 nm, respectively. This can be attributed to the growth of particle sizes and the improvement of crystallinity. Magnetic measurements on the ∼5 nm Fe_3O_4 nanoparticles indicate that the small size particles are superparamagnetic at room temperature. Figure 6(b) shows the hysteresis loops of small size (∼5 nm) Fe_3O_4 nanoparticles measured by SQUID at 5 K and 300 K. It is observed from Fig. 6(b) that ∼5 nm particles are ferromagnetic at 5 K with obvious coercivity of 80.9 Oe, while superparamagnetic at 300 K with no hysteresis. This means that the thermal energy can overcome the anisotropy energy barrier of a single particle, and the net magnetization of Fe_3O_4 nanoparticles in the absence of external field is zero at room temperature.[26] Other than ∼5 nm Fe_3O_4 nanoparticles, the hysteresis loops of the ∼16 nm Fe_3O_4 nanoparticles displays low coercivity of 109 Oe. This is possibly due to the fact that some particles' sizes already exceed the superparamagnetic critical size. It is observed that the saturation magnetization of 5 nm Fe_3O_4 measured by VSM is smaller than that measured by SQUID (300 K). The

reason is that the VSM test time is a few weeks later than SQUID, such a reduction is mainly attributed to the oxidation from Fe_3O_4 to γ-Fe_2O_3, where γ-Fe_2O_3 shows a lower saturation magnetization than that of Fe_3O_4.[27]

In conclusion, the size and shape evolutions of Fe_3O_4 nanoparticles have been systematically investigated by non-injection one-pot and hot-injection methods. The size of Fe_3O_4 nanoparticles is increased by increasing the precursor concentration or extending the duration time in the non-injection one-pot method, or injecting precursor slowly in hot-injection method. The different shapes of Fe_3O_4 nanoparticles can be synthesized when the monomer concentration is controlled by injection. The formation mechanism based on the LaMer model indicates that the nucleation and growth rate are crucial to form size- and shape-controllable Fe_3O_4 nanoparticles, in which the monomer concentration and facet energy might be the dominant factor in our system. The slow rate of injection favors the formation of triangular and cubic-like Fe_3O_4 nanoparticles. The smaller size of Fe_3O_4 nanoparticles show superparamagnetism at room temperature and the saturation magnetization value increases with the increasing size of Fe_3O_4 nanoparticles, which will be suitable for various magnetic applications.

References

[1] Jun Y W et al 2005 *J. Am. Chem. Soc.* **127** 5732
[2] Sun S N et al 2014 *Chin. Phys.* B **23** 037503
[3] Arsalani N, Fattahi H and Nazarpoor M 2010 *eXPRESS Polym. Lett.* **4** 329
[4] Zhu J et al 2015 *Nanoscale* **7** 3392
[5] Liu X W et al 2009 *Cryst. Growth Des.* **9** 197
[6] Wang C, Daimon H and Sun S H 2009 *Nano Lett.* **9** 1493
[7] Zeng T Q et al 2011 *Org. Lett.* **13** 442
[8] Yavuz C T et al 2010 *Environ. Geochem. Health* **32** 327
[9] Yavuz C T et al 2006 *Science* **314** 964
[10] Feng L Y et al 2012 *J. Hazard. Mater.* **217** 439
[11] Xiao S W et al 2015 *Adsorpt. Sci. Technol.* **33** 25
[12] Chikazumi S et al 1987 *J. Magn. Magn. Mater.* **65** 245
[13] Lin C L, Lee C F and Chiu W Y 2005 *J. Colloid Interface Sci.* **291** 411
[14] Madrid S I U et al 2015 *Nanoscale Res. Lett.* **10** 1
[15] Yang X Y et al 2009 *J. Mater. Chem.* **19** 2710
[16] Gupta A K and Gupta M 2005 *Biomaterials* **26** 3995
[17] Pankhurst Q A et al 2003 *J. Phys.* D **36** R167
[18] Xu C J and Sun S H 2009 *Dalton Trans.* **29** 5583
[19] Sun S H and Zeng H 2002 *J. Am. Chem. Soc.* **124** 8204
[20] Ho C H et al 2011 *Chem. Mater.* **23** 1753
[21] Li C H et al 2014 *Nano Res.* **7** 536
[22] LaMer V K and Dinegar R H 1950 *J. Am. Chem. Soc.* **72** 4847
[23] Voorhees P W 1985 *J. Stat. Phys.* **38** 231
[24] Xu Z C et al 2009 *Chem. Mater.* **21** 1778
[25] Song Q and Zhang Z J 2004 *J. Am. Chem. Soc.* **126** 6164
[26] Sun S H et al 2004 *J. Am. Chem. Soc.* **126** 273
[27] Hou Y L, Xu Z C and Sun S H 2007 *Angew. Chem. Int. Ed.* **46** 6329